



NURC

a NATO Research Centre
un Centre de Recherche de l'OTAN



PARTNERING
FOR MARITIME
INNOVATION

Reprint Series

NURC-PR-2008-003

Geoacoustic inversion using multipath pulse shape

Chris H. Harrison, Peter L. Nielsen

September 2008

Originally published in:

Journal of the Acoustical Society of America, Vol. 122, No. 6, December 2007,
pp. 3268-3279.

About NURC

Our vision

- To conduct maritime research and develop products in support of NATO's maritime operational and transformational requirements.
- To be the first port of call for NATO's maritime research needs through our own expertise, particularly in the undersea domain, and that of our many partners in research and technology.

One of three research and technology organisations in NATO, NURC conducts maritime research in support of NATO's operational and transformation requirements. Reporting to the Supreme Allied Commander, Transformation and under the guidance of the NATO Conference of National Armaments Directors and the NATO Military Committee, our focus is on the undersea domain and on solutions to maritime security problems.

The Scientific Committee of National Representatives, membership of which is open to all NATO nations, provides scientific guidance to NURC and the Supreme Allied Commander Transformation.

NURC is funded through NATO common funds and respond explicitly to NATO's common requirements. Our plans and operations are extensively and regularly reviewed by outside bodies including peer review of the science and technology, independent national expert oversight, review of proposed deliverables by military user authorities, and independent business process certification.



Copyright © Acoustical Society of America, 2007.

NOTE: The NURC Reprint series reprints papers and articles published by NURC authors in the open literature as an effort to widely disseminate NURC products. Users should cite the original article where possible.

Geoacoustic inversion using multipath pulse shape

Mark K. Prior,^{a)} Chris H. Harrison,^{b)} and Peter L. Nielsen^{c)}

NATO Undersea Research Centre, Viale S. Bartolomeo 400, 19138 La Spezia, Italy

(Received 20 February 2007; revised 27 June 2007; accepted 27 June 2007)

Experimental data, measured in a shallow water region of the Mediterranean Sea, are used to show that the variation of received intensity with time is well described by existing expressions [Harrison and Nielsen, *J. Acoust. Soc. Am.* **121**, 1362–1373 (2007)]. These expressions indicate that the effect of the sea-water sound speed profile can be neglected for times greater than the peak intensity arrival. Beyond this time, intensity is shown to decay at a rate determined by the seabed acoustic properties in a manner very similar to that for an isovelocity water column. It is shown that a method of determining seabed acoustic properties, previously restricted to isovelocity water columns [Prior and Harrison, *J. Acoust. Soc. Am.* **116**, 1341–1344 (2004)], can consequently be used in the presence of a sound-speed profile. The method relates the decay rate of smeared multipath arrivals to the angular derivative of seabed reflection loss. Two datasets are studied and the method is used to describe average seabed properties and to detect changes in seabed type. The seabed descriptions thus derived are used to predict total received intensity as a function of source-receiver separation. Agreement between the propagation measurements and predictions is shown to be within measurement uncertainties. © 2007 Acoustical Society of America. [DOI: 10.1121/1.2764468]

PACS number(s): 43.30.Ma, 43.20.El [AIT]

I. INTRODUCTION

Underwater acoustic propagation in shallow water environments is critically affected by the composition of the seabed (Kuperman and Jensen, 1980), but it is commonly the case that this composition is not well-enough described in databases to allow accurate prediction of acoustic propagation (Ferla and Jensen, 2002). This limits the accuracy of predictions of sonar system performance and complicates the process of the assessment of the impact of underwater sound on marine mammals (Richardson *et al.*, 1995).

While seabed properties can be assessed by coring and subsequent laboratory analysis (Hamilton, 1980), the difficulty and expense of gathering such information (in quantities sufficient to allow accurate propagation predictions) are prohibitive. An alternative approach is to make controlled measurements of acoustic propagation and to “invert” these measurements to produce estimates of the properties of the seabed in the experimental area (Collins *et al.*, 1992). Such approaches commonly use vertical arrays of sensors to measure acoustic pressure and employ computationally intensive approaches to optimize the match between measurements and the predictions of full-wave propagation models (Gerstoft, 1994).

While these inverse methods are capable of producing good descriptions of seabed acoustic properties, they are generally restricted to research applications by consequence of their use of specialist arrays and computationally intensive analysis schemes. To circumvent this restriction, methods have been proposed (Hermand, 1999; Le Gac *et al.*, 2003; Siderius and Hermand, 1999) in which inversions are per-

formed on broadband acoustic signals, received on more sparse arrays. Such approaches have the potential of being used with simple, cheap, and easily deployable sonar systems. Other attempts to develop acoustic inversion methods not reliant on large-aperture vertical arrays have used towed horizontal arrays (Siderius *et al.*, 2002; Fallat *et al.*, 2005) to gather data that are subsequently inverted using nonlinear schemes.

A more direct method for estimating seabed reflection loss properties (Harrison, 2003; Smith, 1971), based on single-hydrophone measurements of multipath pulse shape, has previously been shown to be capable of showing good agreement with matched-field inversion methods that use a vertical array of hydrophones spanning most of the water column (Prior and Harrison, 2004). The method exploits a simple relationship between seabed reflection loss and the decay rate of acoustic intensity (in dB per second) measured at a receiver located many water depths from a broadband acoustic source. The method’s use of pulse shape, rather than absolute intensity level, means that it does not require the use of calibrated sources or receivers. The method is “direct” in the sense that it does not use inverse methods such as genetic algorithms (Gerstoft, 1994) to search for an optimal environment. Despite this caveat, the method is referred to as an “inversion” because, in common with full-field approaches, it takes acoustic data and “inverts” it to produce estimates of environmental conditions.

While encouraging results have been produced by the method it has so far been based on closed-form expressions for received intensity that are themselves based on an assumption of an isovelocity water column whose validity is questionable in the majority of realistic ocean environments. Recently, however, closed-form expressions for pulse shape, including in-water refraction and lossy reflection at bound-

^{a)}Electronic mail: prior@nurc.nato.int

^{b)}Electronic mail: harrison@nurc.nato.int

^{c)}Electronic mail: nielsen@nurc.nato.int

aries, have been derived (Harrison and Nielsen, 2007) that have been shown to agree with numerical calculations.

This paper describes the use of these expressions to extend the validity of the pulse-shape-inversion method (Prior and Harrison, 2004) to include environments with significant sound-speed gradients present in the water column. It is shown that the original method can be used in an unmodified form with data gathered in the presence of a significant sound speed profile, provided that only the portion of the pulse arriving after the peak intensity is considered. The method is applied to acoustic data gathered in a shallow water region of the Mediterranean Sea to determine average seabed acoustic properties and to identify horizontal changes in seabed type along the source-receiver track.

Section II describes the essentials of the closed-form expressions for the pulse shape, on which the inversion method is based. Pulse shapes predicted by these expressions are then compared with measured data in Sec. III and seabed acoustic properties are estimated from consideration of pulse shapes in Sec. IV.

II. SUMMARY OF THEORY

The full derivation of the closed-form expressions for pulse shape is given elsewhere (Harrison and Nielsen, 2007) and only a summary of those parts relevant to the experimental conditions in which data were gathered is provided here.

The approach considers a constant uniform gradient in the water column. The reflecting surfaces that bound the water column are described as the “low-sound-speed boundary” and “high-sound-speed boundary,” separated by a water depth H and having sound speeds c_L and c_H , respectively. Reflection at the boundaries is lossy with reflection loss proportional to incident angle and with the constants of proportionality at the two surfaces being α_L and α_H . That is, at the low-sound-speed boundary, the reflection coefficient, R_L , is given by

$$R_L = \exp[-\alpha_L \theta_L], \quad (1)$$

where θ_L is the angle at which sound impinges on the boundary and α_L has units of nepers per radian.

The closed-form expressions for pulse shape are derived (Harrison and Nielsen, 2007) by calculating the distribution of intensity with angle and then transforming this into a distribution of intensity with time by consideration of the relationship between the angle of a ray path, its cycle range, and its cycle time. The expressions are general in H , c_L , c_H , α_L , α_H , and the source-receiver range, r .

The experiments considered here had source and receiver in a downward-refracting profile with a smooth sea surface. Thus the low-sound-speed boundary was the only one at which reflection loss was encountered and α_H (which in these circumstances would be a measure of sea surface reflection loss) was set to zero. Furthermore, it was assumed that the travel time of the first arrival was large in comparison to the pulse length, an assumption that is valid for propagation over ranges of more than a few hundred meters.

Under these assumptions, the closed-form expressions predict that the pulse shape is divided into two distinct por-

tions: an initial crescendo and a smoothly decaying trailing edge. The crescendo is formed by the arrival of sound that has followed paths that are reflected at the seabed but are refracted down before they interact with the sea surface. The relationships between angle, travel time, and boundary reflection loss are such that received intensity rises from its value at the time of the first arrival, t_{\min} , until reaching a peak at a later time, t_{\max} , corresponding to the arrival of rays whose path just grazes the sea surface. The width of the crescendo, T_0 , is expressed [Harrison and Nielsen, 2007, Eq. (39)] as

$$T_0 = t_{\max} - t_{\min} = T_L \frac{\delta_{c_{sr}}}{3c_L}, \quad (2)$$

where T_L is the range divided by the sound speed at the lower boundary and $\delta_{c_{sr}}$ is the sound speed difference between source and receiver. The width of the leading edge of the pulse, i.e., the part before the peak intensity arrival, thus increases with source-receiver range and with sound-speed contrast between source and receiver.

For times greater than t_{\max} , sound can only arrive at the receiver via paths that interact both with the sea surface and the seabed and the intensity associated with these paths, I , is calculated by a separate expression that indicates a decay of intensity with a form [Eq. (A19) from Harrison and Nielsen (2007)]:

$$I(\tau)d\tau = \frac{\sqrt{2}}{c_{av}Ht_0^{3/2}\sqrt{\tau}} \exp\left[\frac{-c_{av}\alpha_L\tau}{H}\left(1 + \frac{Hc'}{2c_L}\right) - \frac{c't_0c_{av}\alpha_L}{4c_L}\right]d\tau, \quad (3)$$

where τ is the reduced time, i.e., the time after the peak arrival at time t_0 , c' is the sound speed gradient, and c_{av} is an average sound speed, given by

$$c_{av} = 2 \frac{c_L c_H}{c_L + c_H}. \quad (4)$$

The expression for the pulse shape in the absence of a sound-speed profile, previously derived (Smith, 1971; Harrison, 2003) and already used to deduce seabed reflection properties (Prior and Harrison, 2004), is of the form

$$I(\tau)d\tau = (2t_0)^{-1/2} \frac{\exp\{-\alpha H\tau/c\}}{\sqrt{\tau}} d\tau. \quad (5)$$

The decay rate of logarithmic intensity, after scaling by the square root of τ , given by

$$\frac{d}{d\tau} \{\log[\sqrt{\tau}I(\tau)d\tau]\}, \quad (6)$$

is therefore modified from the isovelocity case only by the use of an average sound speed and by the presence of the multiplier $[1 + (Hc')/(2c_L)]$. The ratio in this multiplier can be estimated to be of the order of 1/100, assuming a value of 30 m/s for the numerator and 3000 m/s for the denominator. The slope of the trailing edge of the pulse is therefore quasi-independent of the sound-speed profile. This quasi-independence arises physically from the fact that the trailing

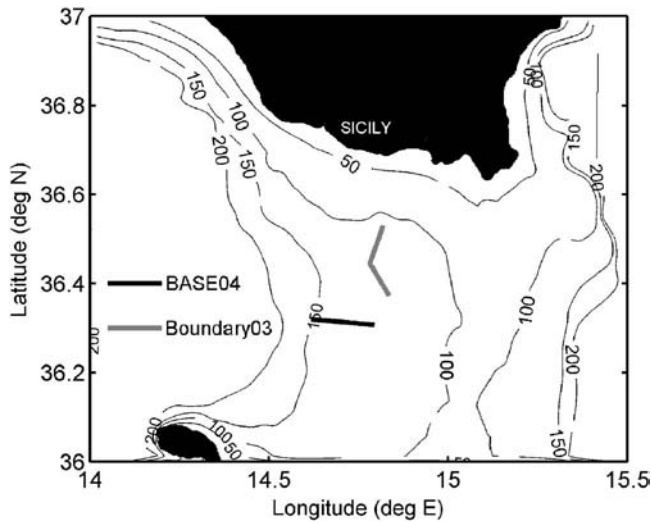


FIG. 1. Map of experimental area. Contours show water depth in meters.

edge of the pulse is made up of steep, nearly straight rays that traverse the entire water column and interact with both boundaries. Such sound is, by definition, only weakly affected by the sound-speed profile.

The pulse shape received in a downward-refracting environment is thus predicted to be made up of a leading edge whose width increases with source-receiver range and source-receiver sound-speed contrast and which ends with the arrival of the peak of the pulse. This is then predicted to be followed by a smooth decay of logarithmic intensity with time after the peak arrival. The rate of decay of intensity, after the peak intensity arrival, is predicted to be independent of source-receiver range and to be insensitive to the details of the seawater sound speed profile.

This predicted behavior is now investigated using measured data.

III. COMPARISON OF MEASURED AND PREDICTED PULSE SHAPES

A. General data description

Acoustic measurements were made during the NURC Boundary 03 and BASE 04 experiments in the Malta Plateau region, south of Sicily, following the paths shown in Fig. 1. These data were examined to investigate the shapes of pulses received after one-way transmission through a shallow water ocean environment. Transmissions were made from a towed source and received on a distant vertical line array (VLA) of receivers.

The signals used in the two experiments were linear frequency modulated and had similar center frequencies and bandwidths representing a considerable fraction of this center frequency.

The source comprised three, free-flooding rings, which, when used simultaneously, formed a transmit beam spread ± 12 deg about the horizontal axis. When only one of the three rings was used during transmission, an effectively omnidirectional beam resulted. Although the one- and three-ring configurations of the source gave different vertical directionalities on transmission, it should be remembered that after

sound has propagated to ranges equivalent to a large number of water depths, most high-angle sound will have been “stripped out” (Harrison, 2003) by repeated bottom reflections. Consequently, the angular spread of sound incident on a receiver at ranges more than 30 water depths (Harrison, 2003) is insensitive to the vertical directivity of the source. This can be illustrated by consideration of a source with a notional Gaussian beam pattern on transmission with width θ_w . The angular distribution of intensity after propagation to a range r in an environment with water depth H and a seabed reflection loss gradient of α is given by (Harrison, 2003):

$$\begin{aligned} I(\theta)d\theta &= \exp\left[-\frac{\theta^2}{\theta_w^2}\right] \exp\left[-\frac{\alpha r\theta^2}{2H}\right] \\ &= \exp\left[-\theta^2\left(\frac{1}{\theta_w^2} + \frac{\alpha r}{2H}\right)\right]. \end{aligned} \quad (7)$$

The bracketed term in the exponential function is effectively independent of θ_w for large r since the second term in the bracket dominates the first.

Source levels of 216 and 206 dB re $1 \mu\text{Pa}$ at 1 m were used for the three- and one-ring configurations, respectively.

Upon reception, signals were correlated with the transmitted signal (i.e., replica correlated) and, since signal bandwidth was never less than 600 Hz, temporal resolution of at least 1.7 ms was achieved. This high temporal resolution ensured that individual paths from source to receiver could be resolved, allowing investigation of the distribution of intensity with time for one-way propagation paths. No beamforming was performed on the data received on the VLA, but intensity data, depth averaged over the VLA, were used in addition to data from single hydrophones.

Although the two experiments were carried out in the same geographic area and used similar signals and sonar equipment, the two experiments covered dissimilar seabed types, had different seawater-sound-speed profiles, and had slightly different source-receiver geometries. Consequently, data from the two experiments are now considered separately.

B. Base 04

Sound speed profiles recorded by expendable bathythermograph casts during the BASE 04 experiment are shown in Fig. 2. Sound speed close to the surface was consistently higher than that at greater depths and sound-speed variations over the entire water column of up to 10 m/s were observed. The greater part of the reduction of sound speed with depth took place in a thermocline region located between 40 and 60 m below the surface.

Source and receiver were placed below this thermocline and sensor depths and pulse properties are summarized in Table I. The vertical extent of the VLA is shown by the straight, black lines in Fig. 2 and the depths of the sources and single-hydrophone receivers are shown by diamond and circular markers, respectively.

The track shown in Fig. 1 for the BASE 04 experiment covers a region in which water depth does not vary significantly from a mean value around 130 m. The seabed in the

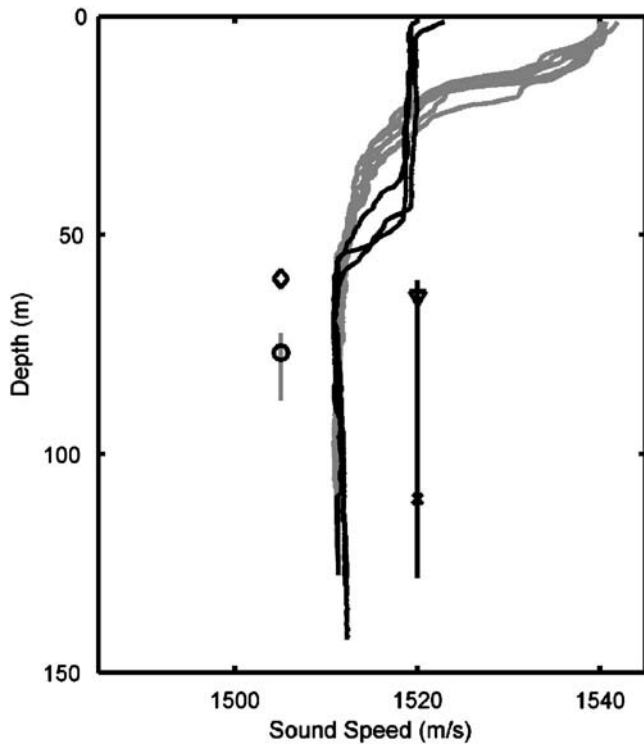


FIG. 2. Sound speed versus depth data deduced from expendable bathythermograph casts taken during the experiments. Gray lines indicate Boundary 03 data; black lines show BASE 04 data. Vertical lines show depths covered by vertical receiver arrays. Diamond shows Boundary 03 source depth, circle shows depths from which single-hydrophone data were taken for Boundary 03 data. Triangle shows BASE 04 source depth; cross shows depths from which single-hydrophone data were taken for Boundary 03 data.

area is silt (Max *et al.*, 1992) but an area of exposed sediment has been identified (Osler and Algan, 1999) and this has been tentatively associated with an area of enhanced reverberation measured in the frequency band of interest here (Prior, 2005). Figure 3 shows the area of enhanced reverberation with the BASE 04 track overlaid. The track is shown to begin in the east, inside the scattering region and to leave it about 15 km from the VLA, marked by the triangle in Fig. 3. In Sec. IVB, we will show that the edge of this region of enhanced reverberation is associated with a change in seabed type, as indicated by changes in pulse shape. The VLA was placed along the line of the track followed, about 3 km beyond the start point.

The pulse shape received on a single element of the VLA for a transmission made from a distance of 19.4 km is shown in Fig. 4 in the form of received intensity in dB *re* 1 μ Pa versus time. The pulse is shown to be made up of a

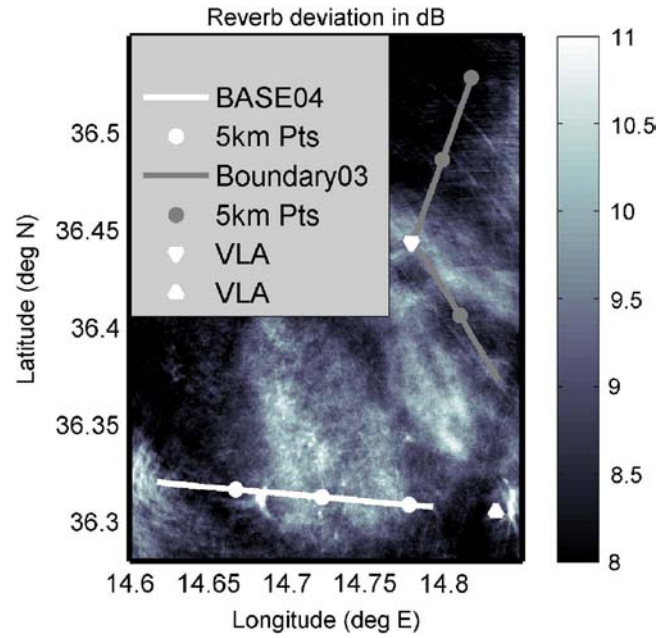


FIG. 3. (Color online) Map showing experimental tracks overlaid on shaded contours of reverberation deviation from an arbitrary reference level. Lighter areas indicate stronger local scattering.

large-amplitude leading edge, followed by a smooth fall-off in the decibel intensity level. The black line in the figure shows a least-square fit to the data of the form given in Eq. (3), i.e., intensity after the peak arrival comprises an exponentially decaying term, divided by the square root of the time after the peak. The argument of the exponential term was estimated by the curve-fitting procedure.

The expanded image of the leading edge, also shown in Fig. 4, reveals that at very short times (~ 10 ms) before the peak, there is evidence of the crescendo of refracted paths predicted by the closed-form expressions for pulse shape (Harrison and Nielsen, 2007).

Figure 5 shows the measured pulse shape for the same transmission but after depth averaging was applied over the VLA. This averaging took the form of summation of the intensity on each hydrophone as a function of time, i.e., incoherent intensity averaging was performed. The fluctuations of intensity with time are shown to be smaller than for the single-phone case and this is a consequence of the averaging process. However, the general features of a spike on the leading edge, followed by a smooth decay of decibel intensity level, are still observed. The data are also shown to be well fitted by the expression given in Eq. (3), indicated by the

TABLE I. Source and receiver characteristics for the BASE 04 and Boundary 03 experiments.

	Source depth (m)	VLA depth coverage (m)	Single receiver depth (m)	No. source rings used	Source level (dB re: 1 μ Pa @ 1 m) ^a	Lower frequency (Hz)	Upper frequency (Hz)	Pulse length (s)
BASE 04	64	60.35-128.3	110.35	3	216	800	1400	1
Boundary 03	60	72.35-87.85	76.85	1	206	700	2000	1

^aValues for source level were averaged over transmitted signal frequency band.

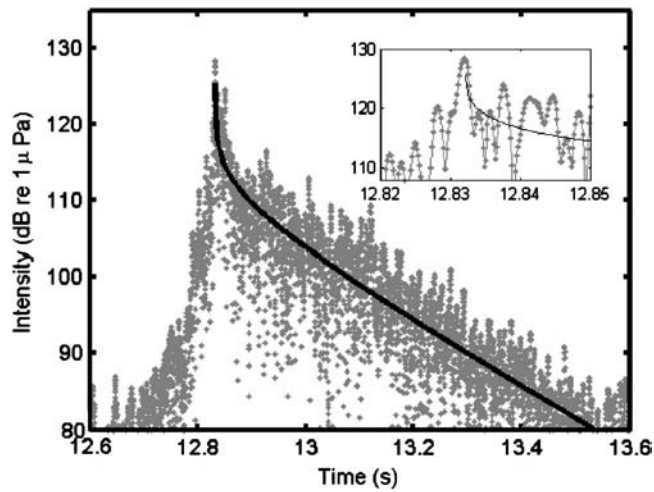


FIG. 4. BASE 04 received pulse shape in the form of intensity versus time for a single receiver located 19.4 km from the acoustic source. Thick black line in main panel shows the predicted pulse shape, fitted to the data. Inset panel shows close-up of arrivals in the vicinity of the intensity peak.

thick black line in Fig. 5. The expanded image of the leading edge of the pulse in Fig. 5 shows evidence of a crescendo before the maximum intensity arrival.

Figure 6 shows an expanded image of the leading edge of a depth-averaged pulse transmitted from a range of 3.2 km. Unlike the longer-range data in Fig. 5, there is no evidence of strong arrivals before the peak of the pulse. While this is consistent with the prediction that the time extent of the crescendo should increase with source-receiver range, the evidence contained in Figs. 5 and 6 cannot be said to provide anything more than slight confirmation of the closed-form expressions relevant to times before the peak intensity of the pulse.

C. Boundary 03

Sound speed profiles recorded by expendable bathythermograph casts during the Boundary 03 experiment are

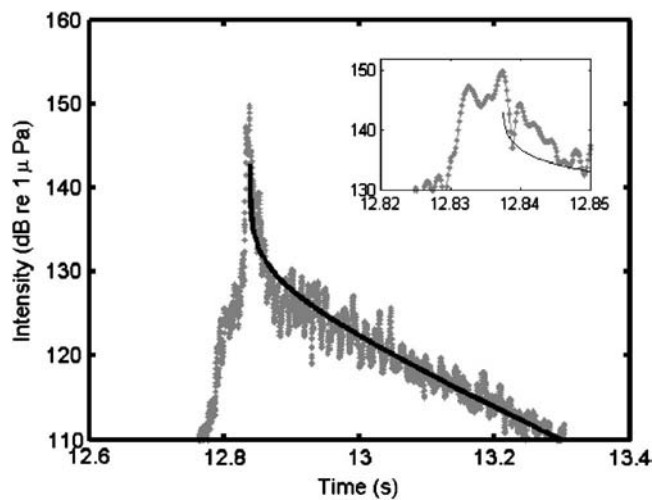


FIG. 5. BASE 04 received pulse shape in the form of depth-averaged intensity versus time. Receiver located 19.4 km from the acoustic source. Thick black line in main panel shows the predicted pulse shape, fitted to the data. Inset panel shows close-up of arrivals in the vicinity of the intensity peak.

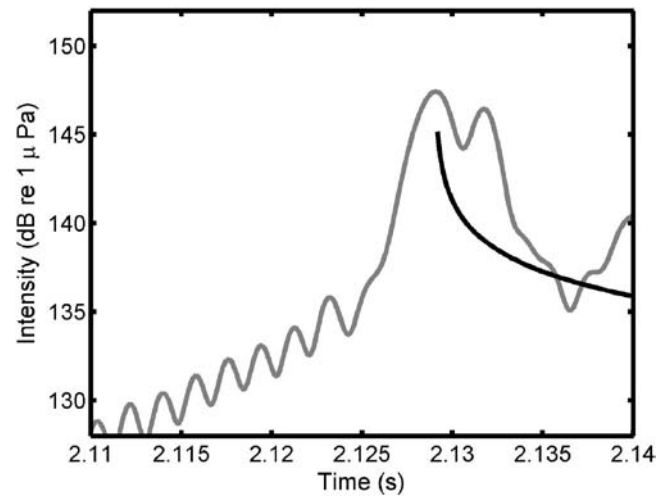


FIG. 6. BASE 04 received pulse shape in vicinity of the intensity peak in the form of depth-averaged intensity versus time. Receiver located 3.2 km from the acoustic source.

shown in Fig. 2. Maximum sound speed was observed at the surface and sound speed decreased steadily with increasing depth from this maximum value of around 1540 m/s to a value of around 1512 m/s at 50 m. Below 50 m, only a slight increase in sound speed with depth was observed.

Source and receiver were placed in the deep layer, and sensor depths and pulse properties are summarized in Table I. The vertical extent of the VLA is shown by the straight, black line in Fig. 2 and the depths of the sources and single-hydrophone receivers are shown by diamond and circular markers, respectively.

The track followed during the Boundary 03 experiment, shown in Fig. 1, was split into two legs. The northern leg followed a track that has previously been identified (Fallat *et al.*, 2005) as having a mud layer overlying a faster sediment below. The mud layer was around 10 m thick at the start of the track but this thickness reduced linearly along the track until, at the end of the track, near the VLA location, the mud layer vanished and the faster sediment was exposed. This boundary has also been associated (Prior, 2005) with the edge of the area of enhanced reverberation shown in Fig. 3.

The southern leg of the Boundary 03 track followed the path along which ambient noise measurements have been used (Harrison, 2004) to produce sub-bottom profiles. There is no evidence of a change of seabed type along this leg.

The pulse received on a single hydrophone for a transmission 9 km distant from the receiver, close to the northern end of the Boundary 03 run shown in Fig. 1, is shown in Fig. 7. The general shape of the pulse is similar to the shapes observed in the BASE 04 data, shown in Figs. 4 and 5, and the upper envelope of the pulse is well described by the form of Eq. (3), as shown by the black line in Fig. 7. The major difference between the data shown in Fig. 7 and those previously seen for the BASE 04 dataset is that the decay of intensity occurs at a much higher rate in the Boundary 03 data. This rapid fall-off of intensity was not limited to the single hydrophone whose data are shown in Fig. 7, and the same behavior was observed in depth-averaged intensity for the same pulse, as shown in Fig. 8.

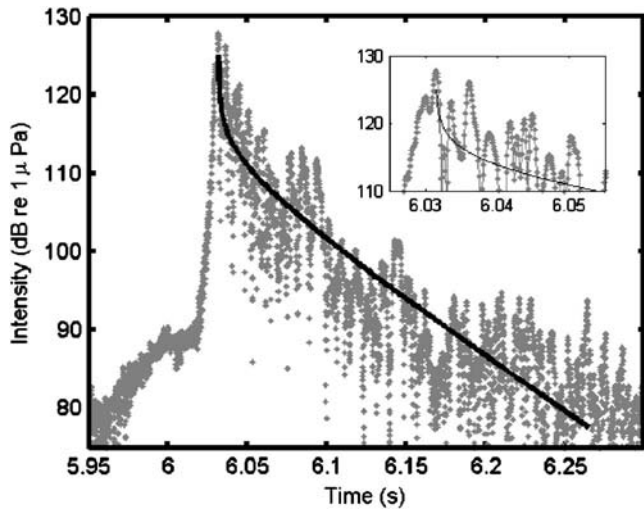


FIG. 7. Boundary 03 received pulse shape in the form of intensity versus time for a transmission made 9 km north of a single-hydrophone receiver. Thick black line in main panel shows the predicted pulse shape, fitted to the data. Inset panel shows close-up of arrivals in the vicinity of the intensity peak.

However, the rapid fall-off was not observed for the southern leg of the Boundary 03 track, as shown in Fig. 9. The figure shows the depth-averaged pulse shape received following a transmission, also 9 km distant from the VLA, and, although the shape of the pulse still follows the form predicted by Eq. (3), the rate of intensity decay is significantly less than for the pulse transmitted at a similar distance north of the VLA.

None of the data in Figs. 7 and 8, or 9 show significant evidence of any crescendo preceding the maximum intensity arrival. This is consistent with the prediction of the closed-form expressions of pulse shape (Harrison and Nielsen, 2007), that the width of the crescendo is proportional to the sound speed difference between source and receiver depths, since the source and receiver were placed at depths at which

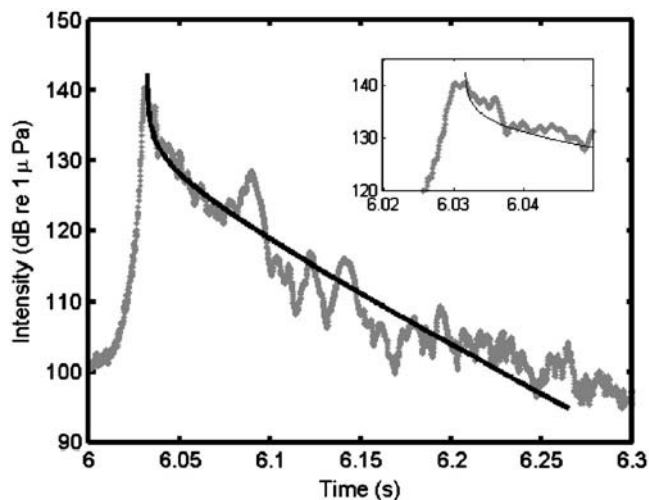


FIG. 8. Boundary 03 received pulse shape in the form of depth-averaged intensity versus time for a transmission made 9 km north of the receiver array. Thick black line in main panel shows the predicted pulse shape, fitted to the data. Inset panel shows close-up of arrivals in the vicinity of the intensity peak.

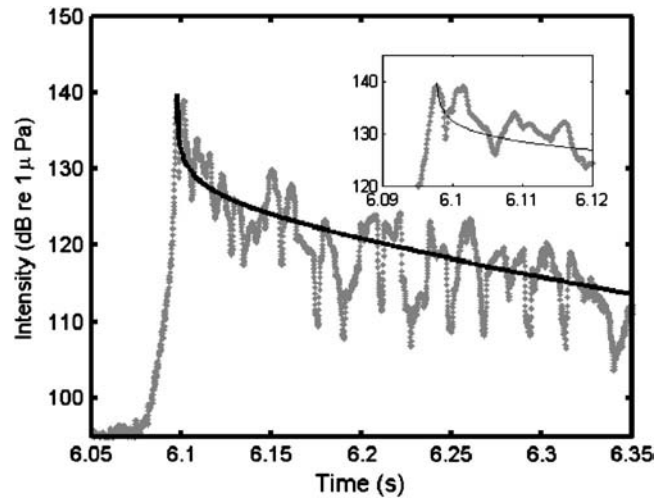


FIG. 9. Boundary 03 received pulse shape in the form of depth-averaged intensity versus time for a transmission made 9 km south-east of the receiver array. Thick black line in main panel shows the predicted pulse shape, fitted to the data. Inset panel shows close-up of arrivals in the vicinity of the intensity peak.

the sound speed differed by only 0.4 m/s. The source and receiver in the BASE 04 data had a sound speed contrast of 0.8 m/s.

D. Summary of comparison of predicted and measured pulse shapes

The acoustic data gathered during the BASE 04 and Boundary 03 experiments allowed examination of the shapes of pulses received after one-way propagation through a shallow water environment over ranges equivalent to many water depths. Good agreement was observed between the measured data and the prediction that pulses would have a trailing edge in which intensity decayed smoothly with time. This good agreement is considered to be supportive of the theoretical predictions made by Harrison and Nielsen (2007).

Only slight evidence was observed of the presence of a crescendo before the peak intensity arrival in the BASE 04 dataset. The Boundary 03 dataset showed no such evidence but this absence is consistent with the closed-form expressions, given the low sound-speed contrast observed between source and receiver depths in the Boundary 03 experiment.

The good agreement between the shape of the trailing edges of measured pulses and the predictions made by the closed-form expressions extends the possibility of using those expressions and data to estimate seabed reflection properties. This estimation process is now described.

IV. ESTIMATION OF SEABED REFLECTION PROPERTIES FROM PULSE SHAPE

A. General description of procedure

Estimates of the seabed near-grazing reflection-loss gradient were made by calculating the function given in Eq. (6). That is, the rate of change of logarithmic intensity with respect to time was calculated, after multiplication by the reduced time variable, τ . The closed-form expression for the pulse shape, Eq. (3), shows that this “rate of decay” is pro-

TABLE II. Geoacoustic parameters for typical sediment types, taken from [Hamilton \(1980\)](#)

Type	Speed (m/s)	Specific gravity	Absorption (dB/λ)	α (Nps/rad)	θ_c (deg)	$r_0/H = 2/(\alpha\theta_c^2)$
Coarse sand	1836	2.03	0.6	0.31	35.22	17.02
Very fine sand	1709	1.88	0.5	0.43	28.63	16.59
Silt	1615	1.74	0.3	0.65	21.75	21.4
Silty clay	1517	1.48	0.1	3.18	8.59	27.9

portional to the seabed near-grazing reflection-loss gradient, α_L . If the bracketed term $[1+(Hc)/(2c_L)]$ in Eq. (6) is assumed to be effectively unity, α_L can be estimated by simply multiplying the rate of decay by the water depth, H , and dividing by the seawater sound speed at the seabed, c_L .

The rate of decay was calculated from the measured data by an automatic algorithm that identified the time of peak intensity arrival. This time was then used to scale out the reduced time, τ . The natural logarithm of the resulting scaled intensity was then calculated and a least-squares-fit was made to this data to extract the rate of decay. The thick, black lines shown in Figs. 4–9 were produced using rates of decay calculated in this way and the figures show that the approach produced good descriptions of the shape of the pulses' trailing edges.

The estimates of seabed acoustic properties produced in this manner are now described for the two experimental datasets.

B. Base 04

Closed-form expressions for pulse shape predict that the slope of the trailing edge of the pulse should not change as source-receiver separation increases beyond a critical range, r_0 , this range being determined by the seabed type ([Harrison, 2003](#)) but being between 15 and 30 water depths for most seabed types. Some typical values are given in Table II. This behavior has been previously observed ([Prior and Harrison, 2004](#)) in the Malta Plateau in a situation where the seawater sound speed profile was effectively isovelocity.

Figure 10 shows the slopes of the trailing edge of pulses measured during the BASE 04 experiment, plotted as a function of source-receiver range. The slope is quantified in two ways: as intensity fall-off in dB per second and as inferred reflection-loss gradient. This latter measure corresponds to the α_L variable in the closed-form expressions and is determined by multiplying the intensity fall-off by the water depth and then dividing by the seawater sound speed at the seabed. Figure 10 shows values derived from single-hydrophone measurements and from data averaged over the entire extent of the VLA.

The data shown in Fig. 10, for ranges less than 15 km, show the behavior predicted by the closed-form expressions, i.e., the slope of the trailing edge of the pulse did not vary with range. The mean value of the intensity fall-off for the single-hydrophone data for ranges less than 15 km is 38 dB/s with a standard deviation of ± 5 dB/s about this mean. The same values for the depth-averaged data are 37 dB/s and ± 3 dB/s. These two values indicate that, while depth averaging reduced the variability of the slopes of the

trailing edge of the pulse, the mean value was effectively the same as that observed for the single-hydrophone data. The reflection-loss gradients corresponding to the measured intensity decays are 0.75 ± 0.09 nepers per radian for the single-hydrophone data and 0.74 ± 0.05 nepers per radian for the depth-averaged data. Inspection of Table II indicates that these values lie between those for silt and silty clay. The seabed in the experimental area has previously been shown to be silt ([Prior and Harrison, 2004](#)) and the values are therefore physically reasonable.

There is no evidence of the previously observed ([Prior and Harrison, 2004](#)) change of trailing-edge slope at very short ranges. However, the minimum range in the dataset (3.5 km) corresponds to 27 water depths and this is not significantly less than the critical limit of 21 water depths predicted for silt, as quoted in Table II. Consequently, the BASE 04 data did not cover ranges short enough to identify the critical range r_0 . Estimates of this range can be used ([Prior and Harrison, 2004](#)) to estimate seabed critical angle and hence sound speed, density, and attenuation, but this procedure could not be followed with the data gathered during the BASE 04 run considered here.

For ranges greater than 14 km the single-hydrophone and depth-averaged data diverge from the behavior exhibited at shorter ranges. The single-hydrophone intensity-gradient data for ranges greater than 14 km had a mean value of

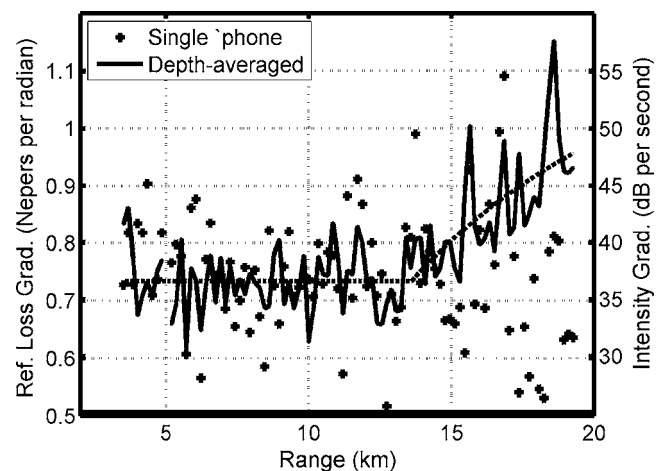


FIG. 10. Rate of decay of intensity deduced from measured pulse shape for BASE 04 dataset. Right-hand y axis gives rate in dB/s. Left-hand y-axis gives the deduced rate-of-change of seabed reflection loss versus angle at grazing incidence. Crosses show data taken from a single hydrophone, solid line shows data taken from intensity depth averaged over the whole array. Dashed line shows a parametric fit to the data calculated assuming that the measured value is an along-track-averaged measure of a range-dependent variable.

36 dB/s and standard deviation about that mean of ± 7 dB/s, indicating no significant change in mean gradient but an increase in variability. The depth-averaged data, however, showed a steady rise at longer range. Inspection of Fig. 3 shows that the 15 km point on the track (indicated by the westernmost circular marker on the BASE 04 track) is in the region where the track leaves the area of enhanced scattering that has been associated (Osler and Algan, 1999) with an area of exposed sediment. The sediment outside the exposed area has previously (Prior and Harrison, 2004) been shown to have a reflection-loss gradient higher than the mean value of 0.74 nepers per radian. It is therefore possible that the changes in behavior observed around 15 km may be explained by a change in the seabed type close to that location.

To investigate this possibility, it was hypothesized that the depth-averaged data represented an along-track-averaged measure of the seabed reflection-loss gradient, with the seabed having a reflection-loss gradient of α_1 from the start of the track to a range R_c , beyond which the seabed reflection-loss gradient changed to a value of α_2 . Under this hypothesis, the measured reflection-loss gradient would be given by

$$\alpha = \frac{1}{R} \int_0^R \alpha(r) dr = \begin{cases} \alpha_1, & R < R_c, \\ \frac{\alpha_1 R_c + \alpha_2 (R - R_c)}{R}, & R \geq R_c, \end{cases} \quad (8)$$

where α is the reflection-loss gradient inferred from the depth-averaged pulse-shape data and R is the range between source and receiver.

The depth-averaged data were fitted with curves of this type and a genetic algorithm (Houck *et al.*, 1995) used to determine values of α_1 , α_2 , and R_c that best matched the data in the sense of minimizing the root-mean-square mismatch between the data and the predictions of the expression given in Eq. (8). Search bounds for R_c were set at the minimum and maximum ranges of the experiment and the two reflection-loss gradients were searched for in bounds between 0 and 5 nepers per radian. The genetic algorithm used a population size of 80 and was run 1001 times so that the repeatability of the method's predictions could be investigated. The lowest mismatch was produced for R_c equal to 13.6 km with α_1 and α_2 equal to 0.734 and 1.49 nepers per radian, respectively.

The error bounds associated with the predicted values for the three parameters were estimated by identifying the range of values returned by the genetic algorithm for each parameter that lay within the best (i.e., lowest mismatch) 10% of the 1001 results. The possible ranges of parameter values thus estimated were $13.2 \leq R_c \leq 14.6$, $0.73 \leq \alpha_1 \leq 0.74$, and $1.4 \leq \alpha_2 \leq 1.8$. It should be noted that these parameter ranges are not unbiased estimates of the uncertainty associated with the estimation of R_c , α_1 , and α_2 (Dosso, 2003) and can only be considered as rough indications of the spread of possible values.

The dashed line in Fig. 10 shows the values of α predicted by Eq. (8), using the best-fit values. The good fit between data and Eq. (8) supports the hypothesis that the seabed type changed around 14 km along the BASE 04 track.

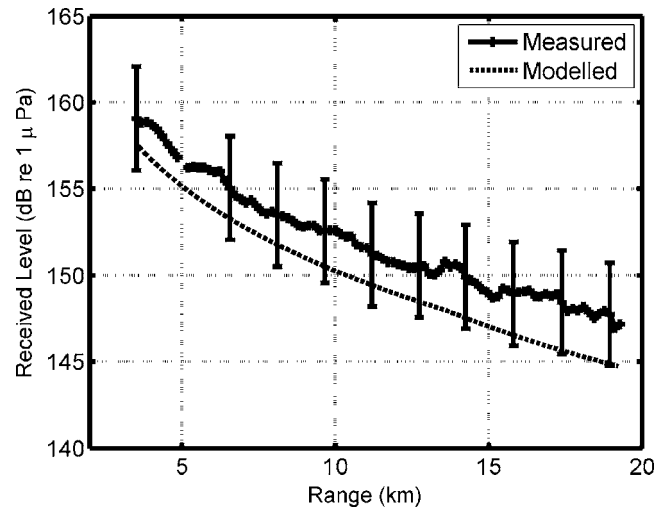


FIG. 11. Time-integrated intensity received as a function of source-receiver range for the BASE 04 dataset. Solid line shows depth-averaged measured data with error bars. Dashed line shows intensity predicted using a simple propagation expression with seabed description data derived from consideration of pulse shape.

Comparison of the genetic algorithm estimate for α_2 with the data in Table II suggests that the seabed inside the area of exposed sediment was more coarse-grained than that outside. This is consistent with the exposed sediment area causing enhanced reverberation, as shown in Fig. 3.

The values of reflection-loss gradient derived from pulse shape can be validated by comparison between total, i.e., time-summed, received intensity predicted using those values and the measured total intensity. Because reflection-loss gradient is determined only from the shape of the pulse, it is independent of the absolute received level, and the comparison between measured and predicted received levels is therefore an independent check, not a circular argument.

The pulse shapes shown in the preceding figures indicated that the majority of the paths between source and receiver were associated with the trailing edge of the pulse and were consequently only weakly affected by the sound speed profile. This allowed the use of a simple expression for intensity, I , measured by a receiver in the mode-stripping region, i.e., at ranges greater than the critical values given in Table II (Harrison, 2003):

$$I = S_l \sqrt{\frac{2\pi}{H\alpha r^3}} \exp[-2\beta r], \quad (9)$$

where S_l is the level of the source, expressed in linear, rather than logarithmic, units, β is the amplitude absorption coefficient (Thorp, 1967), and α is the range-averaged value of reflection-loss gradient, defined in Eq. (8). The absorption coefficient, β , is a function of frequency but a single value, calculated at the center frequency of the transmissions, was used. The intensity predicted by Eq. (9) and the depth-averaged intensity measured on the VLA are shown in Fig. 11. The error bars shown on the measured data are plotted only at ten ranges for clarity but are applicable to all measured values. The ± 3 dB uncertainty shown was calculated by combining an estimated ± 2 dB uncertainty in source level with an independent ± 1 dB uncertainty in receiver calibration.

tion, the two uncertainties being squared, added, and square-rooted before rounding up to an integer decibel value.

The simple formula for the received intensity, Eq. (9), is shown in Fig. 11 to predict levels within the uncertainty associated with the measurements over the entire dataset. The mean difference between measured and predicted levels was 2.1 dB, but the difference between predictions and measurements shows a slight tendency to increase with range. This agreement can be considered to indicate that the estimated values of reflection-loss gradient are reasonable descriptions of the seabed acoustic properties in the region of the BASE 04 experimental track.

It should be noted that the modeled intensity in Fig. 11 includes no dependence on seabed critical angle since the pulse shape data allowed no estimate of this angle to be made. However, noting that the average value of reflection-loss gradient at short range, 0.73, is close to the value associated (Hamilton, 1980; Prior and Harrison, 2004) with silt, the seabed critical angle might be estimated to be around 20 deg, based on a sound speed of 1615 m/s. The correction that must be made to the predicted intensity to allow for this critical angle takes the form (Harrison, 2003) of an error function by which the intensity is multiplied and whose importance decreases with range. For the BASE 04 environmental conditions, this correction is only greater than 1 dB for ranges less than 1.5 km. Any critical angle effects are therefore likely to be small.

In summary, the results from the BASE 04 experiment considered here support the predictions of pulse shape made by the closed-form expressions in that range-invariant slopes of pulses' trailing edges were observed in the BASE 04 data for ranges less than 14 km for both single-hydrophone and depth-averaged data. The divergence from this behavior at ranges greater than 14 km, most clearly observed in the depth-averaged data, is explicable in terms of a change in seabed type around 14 km along the track. The depth-averaged data allow the location and nature of this change to be quantified and the location of the hypothesized change in seabed type matches well with independent evidence. The seabed properties, summarized by a reflection-loss gradient, deduced from the pulse shape were shown to allow a simple expression for received intensity level to produce predictions that agreed with measurements, to within experimental uncertainties.

C. Boundary 03

The difference between the northern and southern legs of the Boundary 03 runs is illustrated in Fig. 12 where the rate of decay of intensity [after the square root term from Eq. (3) has been removed] is plotted as a function of source-VLA distance. The data in Fig. 12 split into two groups with mean values around 25 and 100 dB/s, respectively. The lower values correspond to measurements made along the southern leg of the track while the northern leg of the track yielded the higher values of intensity gradient shown. This is consistent with the presence of a change in seabed type along the two tracks, and the values of the inferred seabed reflection-loss gradient (shown on the left-hand y axis in Fig. 12), when

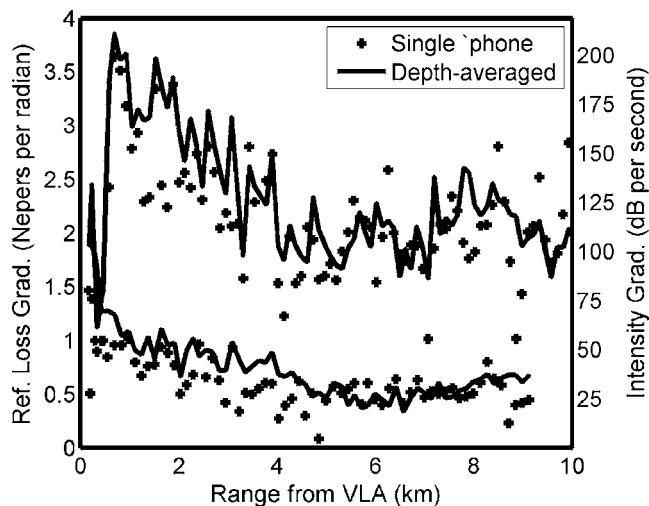


FIG. 12. Rate of decay of intensity deduced from measured pulse shape for Boundary 03 dataset. Right-hand y axis gives rate in dB/s. Left-hand y axis gives the deduced rate-of-change of seabed reflection loss versus angle at grazing incidence. Crosses show data taken from a single hydrophone for transmissions made to the north of the receiver. Circles show data taken from a single hydrophone for transmissions made to the south of the receiver. Solid line shows data taken from intensity depth averaged over the whole array for all transmissions.

compared with the data in Table II, suggest that the seabed to the north was more finely grained than that present along the southern leg. This is consistent with the previous observation (Siderius *et al.*, 2002) of a mud layer along the northern track whose thickness decreased as the VLA position was approached. Within 3 km of the VLA position, the mud layer ended, revealing a layer that has previously (Siderius *et al.*, 2002) been identified as having a higher sound speed than the mud. This change from finer-grained sediments to the north with coarser-grained sediments along the southern leg is consistent with the increase in reverberation observed at the VLA location, shown in Fig. 3.

The short-range ($r < 3$ km) data in Fig. 12 show divergence from the values to which the long-range data converge. This behavior has previously been observed (Prior and Harrison, 2004) for short-range measurements of this kind and is associated with the presence of sound at angles greater than the seabed critical angle. If the range at which the divergence occurs is estimated, then the critical angle of the seabed can also be estimated, (Prior and Harrison, 2004).

This estimation was performed by treating the northern and southern legs of the data separately. For each leg, a 1001-point range variable was produced with values linearly increasing from zero to the maximum range at which a measurement was made within the leg. For each value, r_i , of this range variable, a "score" was calculated to be the number of data points at ranges less than r_i whose values were more than one standard deviation away from the mean value, calculated for measurements made at ranges greater than r_i . The divergence range, r_0 , was then taken to be the range beyond which this score achieved a steady value. The results of this process are shown for the two legs in Figs. 13 and 14.

Figure 13 shows, as a function of source-receiver range, the inferred reflection-loss-gradient values for the northern leg of the Boundary 03 dataset and, in gray, the relative value

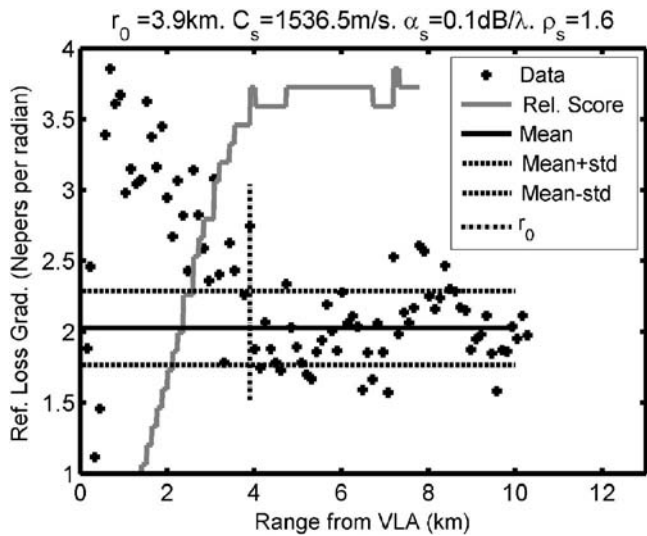


FIG. 13. Reflection-loss gradient data deduced from depth-averaged pulse shape for the northern leg of Boundary 03 dataset, plotted as a function of source-receiver range (crosses). Critical range r_0 deduced as being the shortest range at which the relative score variable (gray line) stopped changing with increasing range. Solid horizontal line shows the mean value of data from ranges greater than r_0 . Dashed lines show mean value \pm one standard deviation about the mean.

of the score used to estimate the location of the range below which the reflection-loss-gradient data diverged from their long-range behavior. A leveling-out of the score is observed at 3.9 km and this value was used to estimate the mean, long-range reflection-loss gradient and the deviation about this mean. These were found to be 2.0 nepers per radian for the mean and 0.3 nepers per radian for the standard deviation and are shown in Fig. 13 by the solid and dashed black lines.

The mean value and the estimate for r_0 were used to estimate the critical angle of the seabed using the expression (Harrison, 2003)

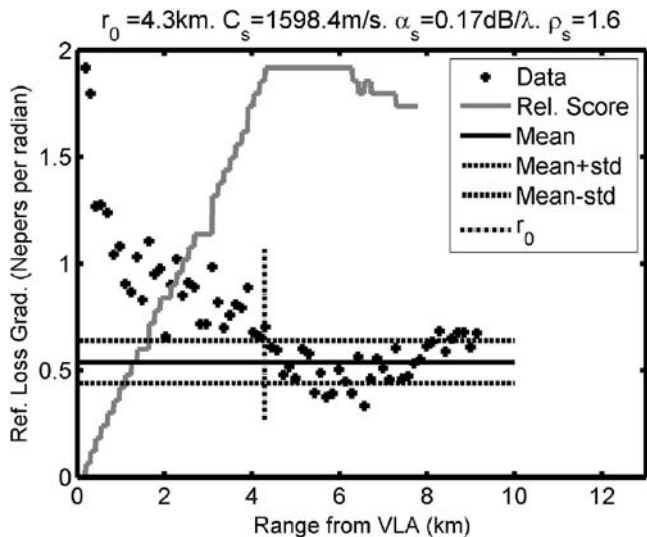


FIG. 14. Reflection-loss gradient data deduced from depth-averaged pulse shape for the southern leg of Boundary 03 dataset, plotted as a function of source-receiver range (crosses). Critical range r_0 deduced as being the shortest range at which the relative score variable (gray line) stopped changing with increasing range. Solid horizontal line shows the mean value of data from ranges greater than r_0 . Dashed lines show mean value \pm one standard deviation about the mean.

$$\theta_c = \sqrt{\frac{2H}{\alpha r_0}}, \quad (10)$$

where θ_c is the critical angle. The critical angle was estimated in this way to be 10.2 deg, corresponding to a seabed sound speed of 1536.5 m/s. This sound-speed value was used to estimate the seabed specific gravity via Hamilton's regression curves (Hamilton, 1978) relating density to sound speed for silt sediments. The resulting value, 1.6, was then combined with the estimated values of sound speed and reflection-loss gradient and [using Weston's expression (Weston, 1971) relating these properties for a fluid, semi-infinite seabed] the seabed attenuation coefficient was estimated to be 0.1 dB per wavelength.

While these values for sound speed, density, and attenuation lie within physical limits for silt sediments, previous surveys (Siderius *et al.*, 2002; Fallat *et al.*, 2005) have suggested that the surficial sediment along the track is more fine-grained with consequently lower sound speed. However, those surveys have also shown that there is significant layering in the seabed along the track and the fine-grained upper sediment lies on top of coarser-grained sediment with higher sound speed. The sediment properties estimated here using consideration of pulse shape therefore probably represent an "effective" sediment whose properties gave near-grazing reflection-loss gradient similar to that obtained from the actual, layered seabed.

Figure 14 shows the inferred reflection-loss-gradient data for the southern leg of the Boundary 03 run, plotted as a function of range, along with the score used to calculate the range at which the data converged to their stable value. The reflection-loss-gradient was found to have a mean of 0.54 nepers per radian with a standard deviation about this mean of 0.1 nepers per radian. The divergence range, r_0 , was estimated to be 4.3 km and this gave estimates for sediment properties of 1598.4 m/s, 0.17 dB per wavelength, and a specific gravity of 1.6. These values are within the range quoted in Table II for silty sediments and are reasonably close to values estimated using matched-field inversion (Siderius *et al.*, 2002) in the vicinity of the experiment (1554.3 m/s, 0.1 dB per wavelength, and 1.8).

While the agreement with previous, matched-field inversion results is encouraging, it is more important that the estimates of seabed properties should allow a good prediction of in-water propagation in the area. To investigate this, the values for reflection-loss gradient were used in conjunction with Eq. (9) to estimate the received level at the VLA. These estimates were compared with the measured data in the same way as for the BASE 04 dataset, previously described. For the northern leg, the water depth varied along the track from 105 m at the start of the track to 128 m at the VLA location. This range-dependent bathymetry was included in the estimates using the concept of an effective depth (Harrison, 2003; Weston and Tindle, 1979) that allows propagation between two points in an environment with a range-dependent bathymetry, $H(r)$, to be predicted using a single, effective water depth, H_{eff} , given by

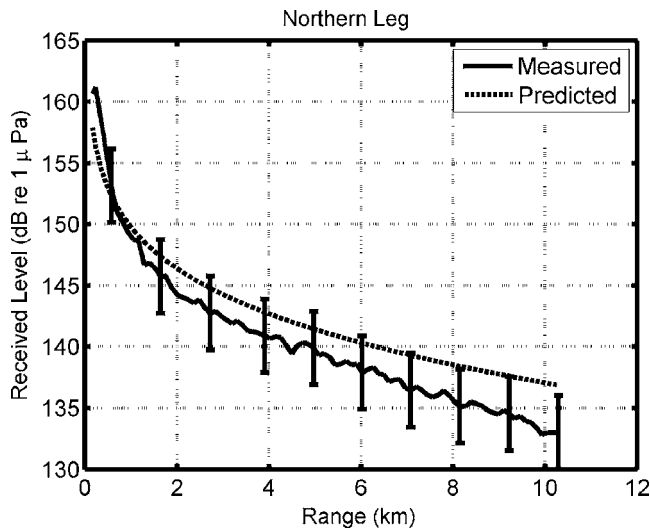


FIG. 15. Time-integrated intensity received as a function of source-receiver range for the northern leg of Boundary 03 dataset. Solid line shows depth-averaged measured data with error bars. Dashed line shows intensity predicted using a simple propagation expression with seabed description data derived from consideration of pulse shape.

$$H_{eff} = \frac{H_r^2 H_s^2}{r} \int_0^r \frac{dr'}{H^3(r')}, \quad (11)$$

where the water depth at the source is H_s and that at the receiver is H_r .

For the southern leg of the run, the water depth varied by less than 3 m over the 10 km extent of the track and the environment was considered range independent.

The received levels predicted and measured for the northern leg are shown in Fig. 15 with error bars on the measured data indicating the uncertainty associated with the measurements. Measured data were averaged over the depth of the array. The predicted levels agreed with the measurements to within the error bars for the majority of the ranges covered, but the difference between the two curves increased with range. Agreement between the measurements and predictions can still be said to be satisfactory since the mean difference between measured and modeled data was 1.9 dB.

Figure 16 shows measured and predicted levels for the southern leg of the Boundary 03 track and agreement between the two curves is similar to the northern leg, with the predictions lying within the error bars on the measurements over the entire 9 km extent of the track. The mean difference between measured and predicted data was found to be 1.7 dB. Also shown in Fig. 16 are some points of the data measured in the northern leg, shifted by $5 \log_{10}(2.0/0.54)$, i.e., shifted by the amount predicted by Eq. (9) to be the consequence of the decrease in reflection-loss gradient between the two legs from 2.0 to 0.54 nepers per radian. The shifted, northern data points are shown in Fig. 16 to agree closely with the southern data points measured at the same ranges. This indicates that the impact on received levels of the change in seabed type was well predicted by Eq. (9) and this is a further indication that the reflection-loss gradient, as deduced from the shape of the received pulse, is a useful predictor of the absolute received level.

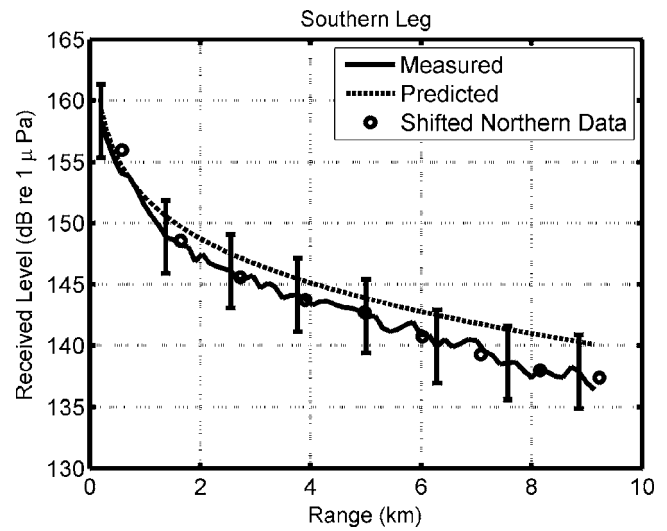


FIG. 16. Time-integrated intensity received as a function of source-receiver range for the southern leg of Boundary 03 dataset. Solid line shows depth-averaged measured data with error bars. Dashed line shows intensity predicted using a simple propagation expression with seabed description data derived from consideration of pulse shape. Circles show data points from the northern leg shifted by an amount (correctly) predicted by closed-form expressions to account for the change in seabed type.

In summary, the data from the Boundary 03 experiment showed that the previously observed change in seabed type at the VLA location was associated with a noticeable change in received pulse shape, as quantified by the slope of the pulses' trailing edge. Values for this slope were used to estimate seabed acoustic properties and these were shown to be comparable to values previously deduced using full, matched-field inversion in the same area. The seabed properties derived from consideration of pulse shape in the Boundary 03 dataset were also shown to allow the prediction of total received intensities at the VLA that agreed with independent measurements, to within experimental uncertainties.

V. CONCLUSIONS

It was shown that the pulse shape measured on a receiver many water depths from an acoustic source was well described by closed-form expressions proposed by Harrison and Nielsen (2007) for times after the arrival of the peak intensity. This shape, as was predicted by the closed-form expressions, was shown to be insensitive to the seawater sound-speed profile.

The rate at which the pulse intensity decayed, in accordance with the theoretical prediction, was used to provide an estimate of the angular gradient of near-grazing reflection loss at the seabed by fitting curves to measured pulse shapes. This method, previously demonstrated in the absence of a significant sound-speed profile, was shown to work even in the presence of vertical variations in sound speed over the water column of around 30 m/s.

The resulting seabed descriptions were shown to be consistent with existing descriptions of the seabed in the experimental area, taken from the literature. Furthermore, it was shown that changes in seabed type along the experimental tracks, previously observed in the study area, were also iden-

tifiable from changes in measured pulse shapes. Thus, not only were mean seabed properties identifiable from the measurements of pulse shape, but the locations of horizontal changes in seabed type were identified and the sizes of these changes were quantified.

The validity of the seabed descriptions derived from inspection of the pulse shape was further demonstrated by comparison between total, time-integrated received levels and the equivalent levels predicted by closed-form expressions. Agreement was found between predictions and measurements to within experimental uncertainties associated with the measurements.

Consideration of the slope of the trailing edges of pulses measured in shallow water therefore provides a possible method for rapidly estimating seabed reflection properties close to grazing incidence, i.e., in the angular regime most important for long-range propagation. The estimated properties are inherently averaged over the entire range from source to receiver and frequency averaged over the entire band of the transmissions. Such averaging is an inevitable consequence of the use of frequency-spread signals in real ocean environments. The averaged values should, however, be useful in all but rare cases which show extremely rapid variation of seabed properties with either acoustic frequency or along-track range. The method can be implemented with a single-hydrophone receiver, such as a standard sonobuoy, and has no need for numerical inversion of the acoustic data. An uncalibrated receiver could be used because of the method's sensitivity to the shape of the pulse, rather than its absolute amplitude. The method is therefore complementary to standard geophysical inversion techniques and could be realized in practical sonar systems without the need for specialist arrays or intensive processing.

ACKNOWLEDGMENTS

We thank the Captain and crew of the *RV Alliance* and the technicians of NURC's engineering department for data collection. The efforts of Georgios Haralabus, the scientist-in-charge of the BASE 04 cruise, are also gratefully acknowledged.

Collins, M. D., Kuperman, W. A., and Schmidt, H. (1992). "Nonlinear inversion for ocean bottom properties," *J. Acoust. Soc. Am.* **92**, 2770–2783.
 Dosso, S. E. (2003). "Quantifying uncertainty in geoaoustic inversion. I. A fast Gibbs sampler approach," *J. Acoust. Soc. Am.* **111**, 129–142.
 Fallat, M. R., Nielsen, P. L., Dosso, S. E., and Siderius, M. (2005). "Geoacoustic characterization of a range-dependent ocean environment using towed array data," *IEEE J. Ocean. Eng.* **30**, 198–206.
 Ferla, C., and Jensen, F. B. (2002). "Are current environmental databases

adequate for sonar predictions in shallow water?" in *Impact of Littoral Environmental Variability on Acoustic Predictions and Sonar Performance*, edited by N. Pace and F. Jensen (Lerici, Italy) (Kluwer Academic Publishers, Dordrecht, The Netherlands).

- Gerstoft, P. (1994). "Inversion of seismo-acoustic data using genetic algorithms and *a posteriori* probability distributions," *J. Acoust. Soc. Am.* **95**, 770–782.
 Hamilton, E. L. (1978). "Sound velocity-density relations in seafloor sediments and rocks," *J. Acoust. Soc. Am.* **63**, 366–377.
 Hamilton, E. L. (1980). "Geoacoustic modeling of the sea floor," *J. Acoust. Soc. Am.* **68**, 1313–1340.
 Harrison, C. H. (2003). "Closed-form expressions for ocean reverberation and signal excess with mode stripping and Lambert's law," *J. Acoust. Soc. Am.* **114**, 2744–2756.
 Harrison, C. H. (2004). "Sub-bottom profiling using ocean ambient noise," *J. Acoust. Soc. Am.* **115**, 1505–1515.
 Harrison, C. H., and Nielsen, P. L. (2007). "Multipath pulse shapes in shallow water: Theory and simulation," *J. Acoust. Soc. Am.* **121**, 1362–1373.
 Hermand, J.-P. (1999). "Broad-band geoaoustic inversion in shallow water from waveguide impulse response measurements on a single hydrophone: Theory and experimental results," *IEEE J. Ocean. Eng.* **21**, 324–346.
 Houck, C., Joines, J., and Kay, M. (1995). "A Genetic Algorithm for Function Optimization: A Matlab Implementation," North Carolina State University, Raleigh, NC, Rep. No. NCSU-IE TR 95-09 (available from site location <http://www.ise.ncsu.edu/mirage/GAToolBox/gaot>).
 Kuperman, W. A., and Jensen, F. B. (1980). *Bottom-Interacting Ocean Acoustics* (Plenum, New York).
 Le Gac, J.-C., Asch, M., Stephan, Y., and Demoulin, X. (2003). "Geoacoustic inversion of broad-band acoustic data in shallow water on a single hydrophone," *IEEE J. Ocean. Eng.* **28**, 479–493.
 Max, M. D., Kristensen, A., and Michelozzi, E. (1992). "Small-scale plio-quaternary sequence stratigraphy and shallow geology of the west-central Malta plateau," in *Geological Development of the Sicilian-Tunisian Platform*, Unesco Reports in Marine Science, Vol. **58**, pp. 117–112.
 Osler, J., and Algan, O. (1999). "A high resolution seismic sequence analysis of the Malta Plateau," SACLANT Undersea Research Centre, La Spezia, Italy. Rep. No. SR-311 (obtainable through national distribution centers, see <http://www.nurc.nato.int/pubs/index.htm>).
 Prior, M. K. (2005). "A scatterer map for the Malta Plateau," *IEEE J. Ocean. Eng.* **30**, 676–690.
 Prior, M. K., and Harrison, C. H. (2004). "Estimation of seabed reflection loss properties from direct blast pulse shape (L)," *J. Acoust. Soc. Am.* **116**, 1341–1344.
 Richardson, W. J., Greene, C. R., Malme, C. I., and Thomson, D. H. (1995). *Marine Mammals And Noise* (Academic, San Diego).
 Siderius, M., Nielsen, P. L., and Gerstoft, P. (2002). "Range-dependent seabed characterization by inversion of acoustic data from a towed receiver array," *J. Acoust. Soc. Am.* **112**, 1523–1535.
 Siderius, M., and Hermand, J.-P. (1999). "Yellow Shark Spring 1995: Inversion results from sparse broadband acoustic measurements over a highly range-dependent soft clay layer," *J. Acoust. Soc. Am.* **106**, 637–651.
 Smith, P. J. (1971). "The averaged impulse response of a shallow-water channel," *J. Acoust. Soc. Am.* **50**, 332–336.
 Thorp, W. H. (1967). "Analytic description of the low-frequency attenuation coefficient," *J. Acoust. Soc. Am.* **42**, 270.
 Weston, D. E. (1971). "Intensity-range relations in oceanographic acoustics," *J. Sound Vib.* **18**, 271–287.
 Weston, D. E., and Tindle, C. T. (1979). "Reflection loss and mode attenuation in a Pekeris model," *J. Acoust. Soc. Am.* **66**, 873–879.

Document Data Sheet

Project No.

<i>Security Classification</i>		
<i>Document Serial No.</i> NURC-PR-2008-003	<i>Date of Issue</i> September 2008	<i>Total Pages</i> 12 pp.
<i>Author(s)</i> Prior, M., Harrison, C.H., Nielsen, P.L.		
<i>Title</i> Geoacoustic inversion using multipath pulse shape		
<i>Abstract</i>		
<i>Keywords</i>		
<i>Issuing Organization</i> NURC Viale San Bartolomeo 400, 19126 La Spezia, Italy [From N. America: NURC (New York) APO AE 09613-5000]		Tel: +39 0187 527 361 Fax: +39 0187 527 700 E-mail: library@nurc.nato.int